HHS Public Access

Author manuscript

Radiat Res. Author manuscript; available in PMC 2023 June 01.

Published in final edited form as:

Radiat Res. 2022 June 01; 197(6): 569–582. doi:10.1667/RADE-21-00181.1.

Mitochondrial Damage Response and Fate of Normal Cells Exposed to FLASH Irradiation with Protons

Ziyang Guo[a,b,c,1],

Manuela Buonanno[a,1],

Andrew Harken[a],

Guangming Zhou[b,2],

Tom K. Hei[a,2]

[a] Center for Radiological Research, College of Physician and Surgeons, Columbia University Medical Center, New York, New York

[b] State Key Laboratory of Radiation Medicine and Protection, School of Radiation Medicine and Protection, Institute of Space Life Sciences, Medical College of Soochow University, Collaborative Innovation Center of Radiological Medicine of Jiangsu Higher Education Institutions, Suzhou 215123, China

[c] Department of Ultrasound Medicine, Peking University First Hospital, Beijing, China

Abstract

Radiation therapy (RT) plays an important role in cancer treatment. The clinical efficacy of radiation therapy is, however, limited by normal tissue toxicity in areas surrounding the irradiated tumor. Compared to conventional radiation therapy (CONV-RT) in which doses are typically delivered at dose rates between 0.03–0.05 Gy/s, there is evidence that radiation delivered at dose rates of orders of magnitude higher (known as FLASH-RT), dramatically reduces the adverse side effects in normal tissues while achieving similar tumor control. The present study focused on normal cell response and tested the hypothesis that proton-FLASH irradiation preserves mitochondria function of normal cells through the induction of phosphorylated Drp1. Normal human lung fibroblasts (IMR90) were irradiated under ambient oxygen concentration (21%) with protons (LET = 10 keV/μm) delivered at dose rates of either 0.33 Gy/s or 100 Gy/s. Mitochondrial dynamics, functions, cell growth and changes in protein expression levels were investigated. Compared to lower dose-rate proton irradiation, FLASH-RT prevented mitochondria damage characterized by morphological changes, functional changes (membrane potential, mtDNA copy number and oxidative enzyme levels) and oxyradical production. After CONV-RT, the phosphorylated form of Dynamin-1-like protein (p-Drp1) underwent dephosphorylation and aggregated into the mitochondria resulting in mitochondria fission and subsequent cell death. In contrast, p-Drp1 protein level did not significantly change after delivery of similar FLASH doses. Compared with CONV irradiation, FLASH irradiation using protons induces

[2] Corresponding authors: Tom K. Hei, Columbia University, VC11-218, New York, NY 10032; tkh1@cumc.columbia.edu; and Guangming Zhou, Soochow University, 199 Renai Road, Suzhou 215123, China; gmzhou@suda.edu.cn.

[1]These authors contributed equally to the manuscript.

minimal mitochondria damage; our results highlight a possible contribution of Drp1-mediated mitochondrial homeostasis in this potential novel cancer treatment modality.

INTRODUCTION

It is estimated that some 65% of tumor patients need radiotherapy (RT) alone or in combination with other treatment modalities (1). The cumulative dose to the tumor is limited by the tolerance of the surrounding healthy tissues. Therefore, there is a need to develop more efficient radiotherapy treatments that would allow dose escalation to the tumor while sparing the normal tissues (2, 3). New radiotherapy approaches including proton and carbon particle (4, 5), image guided radiotherapy, stereotactic body radiotherapy (SBRT) and intensity-modulated radiotherapy (IMRT) (6–8), provide a high-precision, higher dose per fraction and/or high-energy treatment options. However, except for particle therapy due to the presence of the Bragg peak, the toxicity to the normal tissues surrounding the irradiated tumor remains a clinical challenge, and radiation-induced adverse side effects still impact the patient's quality of life (9).

FLASH irradiation involves the ultra-fast delivery of radiation at dose rates several hundred times higher than those currently used in conventional dose rate radiation therapy (CONV-RT: 0.03–0.05 Gy/s) (10). In preclinical studies, FLASH-RT has been shown to be less toxic to normal tissue while achieving similar tumor control as CONV-RT. Such sparing effects have been shown in mouse models of lung, breast, or head and neck cancers (11–13), as well as in higher mammals such as mini-pig and cat patients (14). Following the first report showing that electron FLASH-RT could effectively treat a cutaneous lymphoma in a murine model while sparing the skin from serious late effects (11, 15), there has been tremendous interest in its potential clinical application as well as its radiobiology mechanism(s).

Proton-FLASH studies have been limited by the availability of irradiators that can provide such dose rates (16–19). We used a FLASH irradiator to deliver different dose rates of protons (16, 20, 21) of average linear energy transfer (LET) of around 10 keV/μm, which is comparable to that of the typical spread out Bragg peak (SOBP) of a therapeutic proton beam (21). Our previous studies with normal human lung fibroblasts (IMR90) showed that, compared to conventional dose rates, proton-FLASH irradiation mitigated detrimental long-term biological responses particularly when relatively high doses were used. Specifically, in the progeny of irradiated cells, an increase in dose (20 Gy vs. 10 Gy) and dose rate (1,000 Gy/s vs. 0.05 Gy/s) reduced the number of senescence cells and the expression of the pro-inflammatory molecule TGFβ1 (16). Radiation-induced senescence has been proposed as a potential mechanistic link between radiation-induced metabolic oxidative stress and prolonged tissue injury (9), likely mediated by TGFβ1. However, the precise molecular mechanisms by which FLASH-RT can dramatically reduce adverse side effects in the normal tissues while achieving similar tumor control as CONV-RT remain unclear. Indirect radiation-induced effects mediated by reactive oxygen species (ROS) is one potential mechanism which may account for the FLASH effects (12, 22). Published results have indicated that the FLASH-RT sparing effects in normal tissues are, at least in part, mediated by a lower production of ROS (12, 23). Thus, FLASH-RT may be able to disrupt

and bypass ROS-mediated pathogenic cascades that normally lead to normal tissue damage and associated pathology typically found after conventional irradiation of the tumor (12, 24). Given that the mitochondria are a major source of ROS, which are a natural byproduct of the normal metabolism of oxygen and play an important role in cell signaling and homeostasis (25), we focused in the present study on the effect of FLASH on mitochondria function. Upon exposure to environmental stress (e.g., radiation and toxic metals), mitochondrial morphology changes resulting in mitochondrial dysfunctions (26). The chronic increase in oxidative stress promotes tissue inflammation, senescence, cell death and generation of pro-inflammatory and pro-fibrogenic cytokines.

Drp1 (dynamin-related protein 1) is a large GTPase that controls the process of mitochondrial division and mainly localizes to the cytoplasm (27, 28). Upon activation, Drp1 translocate to the mitochondria through binding to its mitochondrial adaptors, such as Fis1 (29), Mff (30) and MiD49/51 (31) to process fission. Drp1 can stabilize the well-known stress protein p53 and is required for p53 translocation to the mitochondria under conditions of oxidative stress (32). In this article we report that compared to conventional dose rates, protons delivered using FLASH dose rates result in little mitochondria damage characterized by alterations in mitochondrial morphology and functional changes in cells, and that the response is mediated via p53-Drp1 pathway.

MATERIALS AND METHODS

Cells

Normal human diploid lung fibroblasts (IMR90 ATCC CCL-186) were grown in Eagle's Minimum Essential Medium (Cell Gro) supplemented with 12.5% heat-inactivated (56°C, 30 min) fetal bovine serum, 400 mM L-alanyl-L-glutamine, 100 U/ml penicillin and 100 mg/ml streptomycin (Sigma). Lung cancer cells (A549 ATCC CCL-185) were grown in RPMI-1640 medium (Sigma). Both cell lines were maintained at 37°C in a 5% CO_2 humidified incubator. For each experiment the cells were seeded 24 h before irradiation on custom-made 60-mm diameter stainless steel dishes with a 6-μm thick mylar bottom (33, 34). Sham-irradiated cells served as control.

Proton FLASH Generated Using the Track Segment Irradiator

The proton-FLASH irradiations were performed using the RARAF track segment beamline whose design had been previously described (33, 34) and its dosimetry has been characterized previously (20, 35). Briefly, the track segment beamline generated a continuous, uniformly spread ion beams from our HVEE Singletron accelerator through a rectangular beam window that was 6 × 28 mm in dimension. During irradiation the cell dishes are passed over the window in a controlled manner such that the window transit time combined with the beam rate provided the dose required to the cells. The dosimetry (20, 35) is controlled by beam penumbra wipe off monitor apertures whose detection is calibrated to a parallel plate, TE-gas filled ionization chamber for beam rate exiting the window. The wipe-off monitor detection during irradiation controlled the motor speed for the cell dishes passing over the window at a speed commensurate with the beam rate for the desired dose. For FLASH dose rates the window width was reduced to 1 mm to lower dish wheel speeds

for proper exposure times (20). The ion LET was measured with a custom-built ionization chamber (33, 34). In this study, cells maintained under ambient oxygen concentration (21%) were exposed to 4.5 MeV protons (LET = 10 keV/μm) delivered at either 0.33 or 100 Gy/s continuous beams at the beam exit window with cell dishes scanned across the window at set speeds to deliver the desired dose (seconds to milliseconds of exposure on an individual cell basis).

Calorimetric Cell Viability Assay

5×10^4 cells/well were plated into 12-well plates and cultured up to 7 days. The cells were fixed with 10% methanol for 20 min, dried thoroughly either in air or in an oven at 37°C. The colonies were then stained with 0.1% crystal violet for 20 min and washed with distilled water to remove any excess dye. 10% acetic acid was then added to each well to extract crystal violet absorbed by cells and the optical density (OD) at 562 nm was determined using a microplate spectrophotometer (Bio-Rad Synergy 2, Segrate, Italy). For each sample, three replicates were analyzed and three independent experiments were performed.

Cell Viability Using Cell Counting Kit-8 (CCK-8)

5×10^3 cells in 100 μL complete medium were seeded into each well of a 96-well plate and incubated overnight. At designated time points, 10 μL of the CCK-8 reagent (Sigma 96992) was added into each well of the plate and incubated at 37°C for 2 h. The reagent contains the highly water-soluble tetrazolium salt WST-8 [2-(2-methoxy-4-nitrophenyl)-3-(4-nitrophenyl)-5-(2,4-disulfophenyl)-2H-tetrazolium, monosodium salt] that produces a water-soluble formazan dye upon reduction of an electron carrier in the culture medium. The amount of the formazan dye generated by the activity of dehydrogenases in cells is directly proportional to the number of living cells. The optical density (OD) of formazan at 450 nm (OD_{450}) was measured at the microplate spectrophotometer. Cell viability for each dose was calculated as ratio of OD_{450} at that dose divided the OD_{450} of the control. For each sample, three replicates were analyzed and three independent experiments were performed.

Intracellular ROS

CM-H2DCFDA (10 μM, Invitrogen C6827) was added to the cells immediately postirradiation. The dye enters the cells, gets converted into the fluorescent [5-chloromethyl-2′-7′-dichlorofluorescein (DCF)] product by the action of intracellular peroxides. The cells were incubated in the dark at 37°C for 60 min and then seeded into a 96-well plate with black walls and clear flat bottom to measure fluorescence from below at the microplate reader. For each sample three, replicates were analyzed and three independent experiments were performed.

Mitochondrial Morphology

To stain mitochondria, irradiated and control cells were incubated with 100 nM of green fluorescent Mitotracker Green (MTG) (Invitrogen M7514) in PBS for 40 min at 37°C in a 5% CO_2 humidified incubator. The staining solution was then replaced with fresh pre-warmed media and digital fluorescent images of the cells were acquired using a Nikon

confocal microscope (Nikon TE200-C1). Measurements of mitochondrial size and shape in at least 50 cells per sample were quantified with the Mitochondrial Network Analysis (MiNA) toolset using the Image J program (36–38). Briefly, after the "skeleton" of the fluorescent image was created, the toolset recognized how the pixels were spatially related to measure the length of individuals branches and branches networks. The former could be punctated (a single pixel in the "skeletonized" image), rods (unbranched structures with two or more pixels), and large/round structures. Mitochondrial structures with at least a single node and three branches were counted as networks. Inhibition of Drp-1 (or mitochondrial fission) was obtained by treating the cells with Mdivi-1 (50 M in DMSO, Sigma M0199) for 4 h before irradiation (26) (See also Fig. 6A). For each independent experiment (n = 3) at least 50 cells were scored for each sample.

Drp1 and Mitochondria and p53 Co-Localization

Cells were treated with 400 nM MitoTracker Red CM-H2XRos (Invitrogen M7513) for 30 min. Subsequently, they were washed with PBS, fixed with PBS containing 4% paraformaldehyde, and incubated for 10 min in ice-cold 0.3% Triton X-100 (Sigma X100) for permeabilization. After blocking with 1% BSA in PBS for 1 h, the cells were incubated with anti Drp1 (1:500) antibody for 1 h (NB110-55288SS) and secondary anti-rabbit Alexa488 (Invitrogen A-11034). For co-localization with p53, we used the secondary Alexa555 against anti-p53 (1:1000 CST 9282S). For the colocalization analysis only one focal plane was analyzed with a Nikon confocal microscope (Nikon TE200-C1). For each independent experiment (n = 3) the images of at least 20 cells per sample were analyzed by Image J software. Measurements were exported into Excel and graphed with GraphPad Prism 6.0.

Mitochondrial Membrane Potential

We used the JC-1 (5,5′,6,6′-Tetrachloro-1,1′,3,3′-tetraethylbenzimidazolylcarbocyanine Iodide), a cationic, fluorescent, carbocyanine dye to determine mitochondrial membrane potential. After irradiation, cells were incubated with 5 g/ml JC-1 (Biotium 30001) for 20 min at 37°C, washed, and observed immediately with a fluorescence microscope. In cells with intact mitochondrial membrane potential (MMP), the mitochondria fluoresce red with emission at 590 nm and the cytoplasm fluoresces green. In apoptotic and dead cells, the dye remains in its monomeric form and appear green with an emission at 530 nm. For each sample, we acquired 5 fields of view (10×). We analyzed the fluorescence pictures using Image J software. We performed three independent experiments.

Mitochondrial Copy Number

After irradiation (24–48 h), adherent cells were washed twice with pre-cooled PBS and 1 mL of Trizol was pipetted repeatedly and vigorously onto cells to lyse them. The supernatant was centrifuged, and mitochondrial copy number was determined by real-time PCR. 12S rRNA encoded by mt DNA 12S rRNA forward: AGAACACTACGAGCCACAGC reverse: ACTTGCGCTTACTTTGTAGCC) and 18S rRNA/GAPDH (18S rRNA forward GGAGTATGGTTGCAAAGCTG reverse: CGCTCCACCAACTAAGAACG; GAPDH forward: TACTGGTGTCTTCACCACCA and reverse: CAGGATGCATTGCTGACAATC) encoded by nDNA were amplified. Relative quantification of mtDNA/nDNA ratio was

defined as mitochondrial copy number and determined by the comparative threshold cycle (CT) method described previously (39). For each sample three replicates were analyzed and three independent experiments were performed.

Extracellular Oxygen Consumption

We used the extracellular O_2 consumption assay (Abcam ab197243) to measure oxygen consumption rate. After irradiation, 5–6 × 10^5 cells/well in 150 μL culture medium were seeded in a 96-well plate. Fresh culture media (150 μL) was used as blank controls. Reconstituted extracellular O_2 consumption dye (10 μL) was added to each well and fresh culture media (10 μL) added to blank control wells. The fluorescent dye (Ex/Em = 380/650 nm) was quenched by oxygen. Efficient mitochondrial respiration depleted the oxygen in the assay medium, therefore quenching of the fluorescent dye was reduced and the fluorescence signal increased proportionately. The wells were promptly sealed by adding 100 μL pre-warmed high sensitivity mineral oil to limit diffusion of oxygen into the assay medium and two hours later, we used a fluorescence plate reader pre-set at 37°C to measure extracellular O_2 consumption signal at Ex/Em wavelengths of 380/650 nm. For each sample, three replicates were analyzed and three independent experiments were performed.

Luminescent ATP Detection

We used the luminescent ATP detection assay kit (Abcam ab113849) to measure total endogenous levels of cellular adenosine triphosphate (ATP). After irradiation, 1.2 × 10^4 adherent cells/well in 96-well plates were lysed; upon addition of luciferase enzyme and luciferin the ensuing luminescence was measured with the plate reader. For each sample, three replicates were analyzed and three independent experiments were performed.

Western Blot Analysis

At 24 h postirradiation all adherent cells were washed twice with pre-cooled PBS followed by the addition of 60 μL loading buffer for 5 min. Cells were collected with a scraper in a centrifuge tube and lysed by shaking in an ice bath for 15 min. The lysate was centrifuged in a pre-chilled centrifuge at 14,000× *g* for 15 min, then heated at 99°C for 10 min. Lysates were standardized for protein content and resolved by Invitrogen NuPAGE Bis-Tris protein gels (Invitrogen, NP0322BOX). Blots were incubated with the antibodies listed below at the concentration of 1:1,000 (unless otherwise noted) in PBS and visualized by the enhanced chemiluminescence (ECL) procedure. Drp-1 (NB110-55288SS); p-Drp1 (CST 6319S); PTEN (CST 9559S); cytochrome c (ab133504; concentration 1:5000); COX-IV (CST 4850S); LC3A (CST 4599P); LC3B (CST 3868P); cleaved-caspase3 (CST 9662S); P53 (CST, 9282S); Bax (CST 2772S); c-Myc (CST 9402) and β-actin (CST, 8457S). The Western blots were quantified with Image J software. For each protein, we performed three independent experiments.

Apoptosis and Necrosis Analysis

The Apoptosis and Necrosis Quantification Kit (Biotium 30017) allows detecting apoptotic cells (green) and necrotic cells (red) within the same cell population using a fluorescence microscope. At designated time points postirradiation, the cells were washed twice with

PBS. FITC Annexin V (5 μL) and EthD-III (5 μL) were added to 100 μL 1X binding buffer as staining solution. Cells were incubated with the stain for 15 min at room temperature in the dark and then washed with 1X binding buffer 1–2 times before being evaluated under a fluorescent microscope using FITC and Texas Red or Cy3 filter sets. For each independent experiment (n = 3) the images of at least 10 randomly selected fields for each sample were analyzed by Image J software.

Statistical Analysis

All results are reported as mean ± SEM; fold changes were obtained by normalizing the values of each endpoint to the value measured in the corresponding sham-treated samples. All experiments were independently repeated at least three times and for each endpoint we used GraphPad Prism (v5.01) software to carry out statistical analyses. Briefly, for each endpoint, we performed the Shapiro-Wilk normality test to assess how well the data conform to the Gaussian distribution. If the test results were not significant ($P > 0.05$) we used the analysis of variance (ANOVA). If they were significant ($P < 0.05$), suggesting non-normality, we performed nonparametric tests: Kruskal-Wallis rank sum test, followed by pairwise comparisons using Mann-Whitney U tests with Bonferroni correction for multiple comparisons.

RESULTS

Effects of Proton-FLASH Irradiation on Cellular Growth and ROS Level

Recent studies investigating the dependence of the clonogenic survival of IMR90 normal human fibroblasts on the proton dose rate (16) reported a slight increase in survival after exposure to two FLASH dose rates tested (100 and 1,000 Gy/s) relative to cells irradiated at conventional dose rate (0.05 Gy/s), particularly at the highest dose tested (10 Gy). Such results warranted further investigation. As a first step we tested the effects of proton-FLASH irradiation on the cell viability of IMR90 irradiated at a higher dose (15 Gy). As shown in Fig. 1A and B, after proton exposure delivered at 0, 0.33 Gy/s or 100 Gy/s, 5×10^4 cells/well were plated into 12-well plates, and fixed after incubation for 1, 2, 5, or 7 days. At day 7, we found that the relative cell viability of FLASH-RT group was significantly higher than CONV-RT group. These data indicated that protons delivered at FLASH dose rate reduced cell viability in normal lung fibroblasts at a lower level than cells exposed to CONV-RT. The results were confirmed with CCK8-assay, which revealed that up to 12 h after FLASH-RT had a significant protective impact on normal cell proliferation compared with CONV-RT (Fig. 1C). Similar experiments were carried out in lung cancer cells A549 (Fig. S1A and B; https://doi.org/10.1667/RADE-21-00181.1.S1). As opposed to the IMR90, the relative cell viability of lung cancer cells exposed to 15 Gy FLASH-RT was significantly lower than that measured after CONV-RT. These data indicated that FLASH-RT significantly reduces cell viability in a lung cancer cell line while inflicting minimum toxicity to normal lung fibroblasts.

We then investigated radiation-induced oxidative stress immediately after exposure of IMR90 cells to 15 Gy protons delivered at low (0.33 Gy/s) or high (100 Gy/s) dose rates. N-Acetyl-L-cysteine (NAC) (5 mM) was used as a ROS inhibitor. The fluorescence

indicator of oxidative stress CM-H2DCFDA showed that the ROS level increased readily after CONV-RT, but not after FLASH-RT (Fig. 1D). By 40 min, the level of ROS was more than twice that of background level in CONV-RT ($P < 0.01$) whereas there was no significant change in cells exposed to an equivalent dose delivered at FLASH-RT (Fig. 1D). In the presence of NAC, the increase in fluorescence after CONV-RT was completely abrogated suggesting a potential role of ROS in the differential response of normal cells to conventional proton irradiation compared with FLASH irradiation. While CONV-RT increased ROS level in normal cells, there was no significant change after FLASH-RT.

Mitochondrial Dynamics in Response to Proton FLASH-RT

To investigate the mechanisms underlying proton FLASH-RT effects, we determined whether it would affect the mitochondrial dynamics in irradiated normal cells (IMR90) (Fig. 2A). Images of the Mitotracker green dye showed that mitochondria mainly exhibited elongated and tubular morphology in a perinuclear pattern in the control group. In contrast, irradiated cells showed multiple mitochondrial network abnormalities in CONV-RT group in that the mitochondria had a diffused and disorganized pattern. In cells exposed to an equivalent proton-FLASH dose the mitochondrial exhibited a morphology similar to the non-irradiated control cells (Fig. 2A). The mitochondrial network abnormalities indicated that CONV-RT and FLASH-RT elicited different mitochondrial damage in normal cells. Using Image J software, we next quantified the mitochondria size and length (36). The mean mitochondrial length in IMR90 cells exposed to CONV-RT decreased from 2 μm to 1.5 μm in irradiated cells ($P < 0.001$); such decrease remained constant for the 25 min period examined (Fig. 2B). In contrast, the mitochondrial morphology in the A549 tumor cells was vastly different from the normal lung fibroblasts, with clear aggregates of shortened mitochondria (Fig. S1C and D; https://doi.org/10.1667/RADE-21-00181.1.S1). The perinuclear distribution of the mitochondria in both CONV-RT and FLASH-RT groups was lost with little difference between the irradiated groups. Furthermore, mitochondrial length in irradiated A549 cells shortened significantly in both the irradiated groups ($P < 0.01$) (Fig. S1C and D; https://doi.org/10.1667/RADE-21-00181.1.S1).

Mitochondria maintain their shape, distribution, and size through coordinated cycles of fission and fusion. Such “mitochondrial dynamics” is largely controlled by the fission protein Drp1, a large GTPase required for p53 translocation to the mitochondria under conditions of oxidative stress (32). Therefore, we investigated Drp-1 expression in IMR90 cells exposed to 15 Gy of protons delivered as CONV-RT and FLASH-RT. We found that CONV-RT not only promoted a higher expression of Drp-1 in mitochondria (Fig. 2C and E), but it also co-localized with p53 (Fig. 2D and F) to likely result in mitochondria fission and subsequent cell death. In contrast, there was no significant change in Drp-1 expression after similar FLASH doses. Collectively, these results indicated that FLASH-RT induced little damage on mitochondrial dynamics compared to CONV-RT in irradiated normal cells.

Effect of FLASH-RT on Mitochondrial Functions

To assess mitochondrial functions in normal cells exposed to 15 Gy of protons delivered at different dose rates, we evaluated mitochondrial membrane potential (MMP) using JC-1 dye that exhibits MPP-dependent accumulation in mitochondria, characterized by

a fluorescence emission shift from a monomeric green (~529 nm) to a J-aggregate red (~590 nm). Consequently, mitochondrial depolarization is indicated by a decrease in the red/green fluorescence intensity ratio. As shown in Fig. 3A and B, FLASH-RT induced slight changes in MMP, while CONV-RT led to a significant decrease in the red/green fluorescence intensity ratio, indicative of a decline in mitochondrial health.

Mitochondrial copy number is another marker of the degree of mitochondrial damage (39) and is expressed by the ratio of 12S rRNA/GAPDH. Compared to the FLASH-RT cells, CONV-RT cells showed a significant decrease ($P < 0.05$) in mitochondrial copy number (Fig. 3C). This was associated with a lower oxygen consumption in proton-irradiated normal cells delivered using CONV dose rate compared to controls and FLASH-irradiated cells at 2 h postirradiation (Fig. 3D).

Total levels of cellular ATP can be used to assess the mitochondrial bioenergetic state of normal cells. Compared to control the concentration of ATP decreased by 30.2% after CONV-RT ($P < 0.01$), but only 17.5% after FLASH-RT, although it remained statistically significant ($P < 0.05$). Such decrease could be reversed by the Drp1 inhibitor Mdivi-1 (Fig. 3E and F). Therefore, compared to unirradiated cells CONV-RT affected mitochondrial functions to a greater extent than FLASH-RT.

Protein Expression and Mitochondrial Network Abnormalities

To clarify the possible link between mitochondrial network abnormalities and cell outcome we examined the expression of mitochondrial fission protein and other cellular proteins critical for mitochondrial functions after FLASH-RT in normal cells. Figure 4A shows representative Western blots of several proteins relevant for mitochondrial network functions 24 h after either 1.5 or 15 Gy proton irradiations delivered at a dose rate of 0.33 Gy/s or 15 Gy of protons delivered at 100 Gy/s. Figure 4B–J show the average protein expression from a minimum of three independent experiments. Analysis of the phosphorylated form of Dynamin-1-like protein (p-Drp-1 at Ser 637) and PTEN (Fig. 4B) revealed that their expressions after CONV-RT underwent a dose dependent decrease which could lead to mitochondrion disequilibrium, redox imbalance, and cell death. In contrast, neither protein showed a significant change relative to control after similar FLASH dose (Fig. 4B). Correspondingly, cytochrome c protein expression showed a dose-dependent decrease with CONV-RT compared to a slight increase with FLASH-RT, relative to control (Fig. 4C). We also found analogous results for the autophagy proteins LC3A and LC3B protein levels (Fig. 4D).

While p53 expression was uniformly stimulated in all irradiated groups relative to controls (Fig. 4E), the expression of c-myc was reduced only after conventional high-dose irradiation (15 Gy) (Fig. 4F). Finally, while expressions of both Caspase 3 and Bax showed a slight increase in all irradiated groups relative to controls (Fig. 4H and J), the expression of cleaved-Caspase-3 (Fig. 4I) was similar to the pattern of c-myc with no change in cells exposed to conventional 15 Gy proton-radiation treatment. In contrast, cells exposed to 1.5 Gy of protons using either CONV-RT or 15 Gy FLASH-RT, there was a twofold increase in cleaved-Caspase-3 expression ($P < 0.001$).

These results indicate that compared to protons delivered at relatively low dose rates, proton FLASH-RT had little effect on normal mitochondrial fission and function in normal cells. Our results also suggest that the proton dose rate influences the mode of cell death.

The Fate of Proton-FLASH Irradiated Normal Cells

We next determined the incidence of apoptosis and necrosis in normal IMR90 cells exposed to either CONV-RT and FLASH-RT using AnnexinV-FITC and Et-DIII staining. Four hours after CONV-RT largely resulted in necrotic cell death (Fig. 5A and C), while FLASH-RT mainly led to apoptosis (Fig. 5A and D). The effect was transient (Fig. 5E–H). Since apoptosis is usually regarded as an active programmed process of autonomous cellular dismantling that avoids eliciting inflammation whereas necrosis has been described as passive, accidental cell death resulting from environmental perturbations with uncontrolled release of inflammatory cellular contents (40), it is not unexpected that FLASH-RT indeed resulted in apoptosis (Fig. 5A and D) and possibly autophagy (Fig. 4A and D); these processes remove damaged cells and protect the cells by reducing the production of inflammatory cytokines. In contrast, CONV-RT mainly induced cell necrosis (Fig. 5A and C).

FLASH-RT Leads to Mitochondrial Dysfunction after Mdivi-1 Treatment

To investigate the involvement of Drp-1 on cell survival and mitochondria integrity and their dependence on the proton dose rate, cells were pretreated with the specific inhibitor of Drp-1, Mdivi-1 (41). In fact, Drp-1 protein level significantly decreased at 2 and 4 h after Mdivi-1 treatment (Fig. 6A and B). After 15 Gy proton-irradiation delivered at 0, 0.33 Gy/s or 100 Gy/s 5×10^4 IMR90 normal cells/well were plated into 12-well plates and fixed up to 4 days afterward. At days 3 and 4, we found that the relative cell viability after Mdivi-1 treatment was similar in FLASH-RT and CONV-RT cells (Fig. 6C and D). The results were further confirmed using the CCK-8 assay, which showed that the significant protective impact of FLASH-RT on cell proliferation was abrogated by pretreatment with Mdivi-1 (Fig. 6E).

We next determined radiation-induced oxidative stress immediately after 15 Gy proton irradiation delivered at low (0.33 Gy/s) or high (100 Gy/s) dose rates with or without pretreatment with Mdivi-1 for 4 h. Analysis of the CM-H2DCFDA dye revealed that the ROS level increased within 40 min after CONV-RT, but not after FLASH-RT (Fig. 6F). The experiments were repeated in the presence of the antioxidant NAC to confirm that the detected fluorescence signal was due to the generation of ROS (Fig. 6F); indeed, NAC abrogated the ROS-mediated fluorescence observed after CONV-RT.

As shown in Fig. 4A and B, CONV-RT reduced expression of p-Drp1 and led to mitochondria damage and cell death. In contrast, p-Drp1 protein level did not significantly change after similar FLASH doses. However, this could be circumvented by inhibiting Drp-1. Image analysis showed that mitochondria mainly exhibited elongated and tubular morphology in the control cells. However, after suppression of Drp-1 by Mdivi-1, the cells showed multiple mitochondrial network abnormalities after FLASH-RT and CONV-RT (Fig. 6G and H). Similarly, there were no significant changes in the co-localization of

Drp-1 and mitochondria in the presence of Mdivi-1 (Fig. 6I and J), nor in Cox-IV and cytochrome c proteins level after either FLASH-RT or CONV-RT (Fig. 6K–N). These results suggest a role for Drp-1 in the differential effects, in terms of cell proliferation and mitochondria functions, measured in FLASH irradiated normal cells compared to CONV irradiated normal cells.

DISCUSSION

Our previous studies investigated in vitro short- and long-term biological effects in normal skin fibroblasts exposed to protons delivered at either conventional or with FLASH dose rates (16). In this present study, we extended the work to probe the status of mitochondrial health after proton irradiation at dose rates of 0.33 Gy/s or 100 Gy/s. We confirmed that compared to cells exposed to protons delivered with CONV-RT under ambient oxygen concentration (21%), exposure to protons delivered with FLASH-RT preserved survival (16, 20) as well as mitochondrial functions of normal but not of cancer cells (Fig. 1 and S1). The role of oxygen concentration in the manifestation of FLASH effects in terms of cell survival is still the subject of debate as it may be dependent on the cell type. In the case of cancer cell lines in particular, while for DU145 prostate cancer cells the FLASH effect manifested only at low oxygen concentration (42), other cancer cell lines would show a FLASH effect under normoxic conditions (43). The magnitude of the effect was cell dependent.

There is evidence that conventional-dose rate irradiation induces mitochondrial damage (44) such as mtDNA damage (45), copy number and supercoiling changes (46) as well as a decrease in oxidative phosphorylation activity and oxygen consumption (39). While exposure to conventional 15 Gy proton-radiation induced an increase in ROS (Fig. 1D) and mitochondria dysfunctions (Figs. 2 and 3), of cells FLASH irradiated did not generate an excess in ROS (Fig. 1D); it rather preserved mitochondria structure and copy number, and maintained mitochondrial membrane potential, ATP release, and oxygen consumption at levels similar to those measured in unirradiated cells (Figs. 2 and 3). In contrast, in cancer cells exposure to protons delivered with either CONV or FLASH doses negatively affected mitochondria integrity (Fig. S1; https://doi.org/10.1667/RADE-21-00181.1.S1).

Mitochondria morphology, number, size and positioning within the cytoplasm are coordinated by fission and fusion events (47). One protein involved in such mitochondria dynamics is Drp-1 (48). In normal cells exposed to conventional dose we measured an increased expression of Drp-1, which also localized with p53 to result in mitochondria fission and subsequent cell death (Fig. 2C and D). Similarly, using a single particle microbeam, our studies have shown that targeted cytoplasmic irradiation of human small airway epithelial cells using alpha particles resulted in activation of Drp-1 within 30 min postirradiation (39). In contrast, there was no significant change in Drp-1 expression after similar doses delivered at FLASH dose rate. Moreover, the damaging effects measured in the mitochondria of normal cells exposed to conventional-dose radiation were abrogated when the cells were irradiated in the presence of Mdivi-1, an inhibitor of Drp-1, implicating a possible contribution of this protein in the preservation of normal cells exposed to FLASH dose rates (Fig. 3D and F).

Recent studies showed that mitochondrial dysfunction induced by targeted cytoplasmic irradiation resulted in the activation of autophagy, which degraded dysfunctional mitochondria to maintain cellular energy homeostasis (49). In addition, the autophagic process was oxyradical dependent and required the activity of Drp1. In this study, the protein expression of the autophagy proteins LC3A and LC3B showed a dose-dependent decrease with CONV-RT compared to a slight increase with FLASH-RT, relative to control (Fig. 4A and D). This could partly explain why FLASH irradiation induces little or no mitochondria damage comparing to the CONV irradiation.

Phosphorylation of Drp1 at serine 637 inhibits fission and protects mitochondria from autophagosomal degradation during nutrient deprivation (50) and cell death (51, 53). In this study we showed that, as opposed to FLASH-RT, exposure of normal cells to 15 Gy proton CONV-RT reduced the expression of p-Drp-1 (Ser 637) (Fig. 4A and B). These results indicate that compared to CONV-RT, exposure of cells to FLASH-RT does not induce Drp1 localization from cytoplasmic to mitochondria as well as mitochondrial fragmentation. A possible contribution for Drp-1 in the differential effects measured in normal cells exposed to protons delivered at FLASH-RT compared to CONV-RT was confirmed when the cells were irradiated in the presence of the mitochondrial division inhibitor Mdivi-1 (Fig. 6).

Exposure of normal cells to ionizing radiation affects the expression of numerous proteins such as PTEN, PARP, and p53 (53). Here we investigated how the proton dose rate might affect their expression (Fig. 4) including those involved in cell death (autophagy, apoptosis, and necrosis) (Figs. 4 and 5). We found that CONV-RT mainly resulted in necrotic cell death, whereas FLASH-RT mainly led to transitory apoptosis (Fig. 5) or autophagy (Fig. 4 A and D), suggesting that proton FLASH-RT may favor a death modality of the initially damaged cells that, as opposed to necrosis, does not promote the production of inflammatory cytokines. The type of cell death after FLASH vs CONV irradiations may also depend on the cell oxygen concentration during exposure. Recently, in vitro studies of FLASH effects of laser-driven proton beams in cells exposed under normoxic conditions or when hypoxia was mimicked with $CoCl_2$ have shown that FLASH-RT induced apoptosis and necrosis in normal fibroblasts may be time- and oxygen-concentration dependent and are related to mitochondria dysfunctions (54).

Interestingly, c-myc activation induces apoptosis after stabilization of p53 (40). Based on our results, although p53 expression was uniformly stimulated in all irradiated groups relative to controls (Fig. 4E), c-myc was induced in cells FLASH irradiated but not after conventional irradiation (Fig. 4F). This might have resulted in the induction of apoptosis measured in FLASH-RT group at 4 h postirradiation (Fig. 5D) but not in CONV-RT group (Fig 5C).

Based on our collective results showing that compared to CONV-RT, FLASH-RT resulted in a dramatic reduction of mitochondria damage, we propose the following mechanistic model (Fig. 7): Exposure to protons delivered at conventional dose rates induced p-Drp1 to undergo dephosphorylation and Drp1 to be located in mitochondria, which eventually led to mitochondrion damage and cell necrosis. In contrast, p-Drp1 protein level did not significantly change after similar doses delivered at FLASH dose rates.

Our results highlight the critical involvement of mitochondria in the differential effects elicited in normal cells proton irradiated at CONV vs. FLASH dose rates. Our data support a novel role of Drp1-mediated mitochondrial homeostasis in FLASH irradiation. They open the field to investigation of Drp1-mediated mitochondrial functions in different normal cell lines as well as their cancer cell line counterparts exposed to FLASH dose rate. Studies on the relationship of Drp1-mediated mitochondrial homeostasis and FLASH irradiation under different oxygen concentrations are warranted using both in vivo and in vitro models. In addition, detailed time course studies for all the endpoints presented in this study will further clarify the impact of the dose rate of protons on mitochondria structure and functions.

Supplementary Material

Refer to Web version on PubMed Central for supplementary material.

ACKNOWLEDGMENTS

This work was supported by a grant from National Cancer Institute 1U01CA236554 and from a pilot grant from the Department of Radiation Oncology at Columbia University Irving Medical Center. The statistical assistance provided by Dr. Igor Shuryak was greatly appreciated. Data sharing statement: Columbia University Irving Medical Center and the authors fully endorse the Public Health Service's goals regarding the sharing of data and unique research resources within the scientific community. These will be achieved via: i) publication of our research findings in peer-reviewed journals, and ii) communication at research meetings, workshops and conferences. In addition, the data will be made available to the public by posting on the laboratory website of the corresponding author: https://www.crr.columbia.edu/profile/tom-k-hei-phd.

REFERENCES

1. Citrin DE. Recent Developments in radiotherapy. NEJM. 2017; 377(22):2200–1.
2. Bentzen SM. Preventing or reducing late side effects of radiation therapy: radiobiology meets molecular pathology. Nat Rev Cancer. 2006; 6(9):702–13. [PubMed: 16929324]
3. Yarnold J, Brotons MC. Pathogenetic mechanisms in radiation fibrosis. Radiother Oncol. 2010; 97(1):149–61. [PubMed: 20888056]
4. LaRiviere MJ, Santos PMG, Hill-Kayser CE, Metz JM. Proton therapy. Hematol. Oncol. Clin. North Am. 2019; 33(6):989–1009. [PubMed: 31668216]
5. Kamada T, Tsujii H, Blakely EA, Debus J, De Neve W, Durante M, et al. Carbon ion radiotherapy in Japan: An assessment of 20 years of clinical experience. Lancet Oncol. 2015; 16(2):e93–e100. [PubMed: 25638685]
6. Suppli MH, Munck Af Rosenschold P, Dahl B, Berthelsen AK, Engelholm SA, Pappot H. Premature termination of a randomized controlled trial on image-guided stereotactic body radiotherapy of metastatic spinal cord compression. Oncologist. 2020; 25(3):210–e422. [PubMed: 32162821]
7. Liu R, Buatti JM, Howes TL, Dill J, Modrick JM, Meeks SL. Optimal number of beams for stereotactic body radiotherapy of lung and liver lesions. Int J Radiat Oncol Biol Phys. 2006; 66(3):906–12. [PubMed: 16904842]
8. Lee N, Xia P, Quivey JM, Sultanem K, Poon I, Akazawa C, et al. Intensity-modulated radiotherapy in the treatment of nasopharyngeal carcinoma: an update of the UCSF experience. Int J Radiat Oncol Biol Phys. 2002; 53(1):12–22. [PubMed: 12007936]
9. De Ruysscher D, Niedermann G, Burnet NG, Siva S, Lee AWM, Hegi-Johnson F. Radiotherapy toxicity. Nat Rev Dis Primers. 2019; 5(1):13. [PubMed: 30792503]
10. Bourhis J, Montay-Gruel P, Gonçalves Jorge P, Bailat C, Petit B, Ollivier J, et al. Clinical translation of FLASH radiotherapy: Why and how? Radiother Oncol. 2019; 139:11–7. [PubMed: 31253466]

11. Favaudon V, Caplier L, Monceau V, Pouzoulet F, Sayarath M, Fouillade C, et al. Ultrahigh dose-rate FLASH irradiation increases the differential response between normal and tumor tissue in mice. Sci Transl Med. 2014; 6(245):245ra93.
12. Montay-Gruel P, Acharya MM, Petersson K, Alikhani L, Yakkala C, Allen BD, et al. Long-term neurocognitive benefits of FLASH radiotherapy driven by reduced reactive oxygen species. PNAS 2019; 116(22):10943–51. [PubMed: 31097580]
13. Soto LA, Casey KM, Wang J, Blaney A, Manjappa R, Breitkreutz D, et al. FLASH irradiation results in reduced severe skin toxicity compared to conventional-dose-rate irradiation. Radiat Res. 2020; 194(6):618–24. [PubMed: 32853385]
14. Vozenin MC, De Fornel P, Petersson K, Favaudon V, Jaccard M, Germond JF, et al. The advantage of flash radiotherapy confirmed in mini-pig and cat-cancer patients. Clin Cancer Res. 2019; 25(1):35–42. [PubMed: 29875213]
15. Bourhis J, Sozzi WJ, Jorge PG, Gaide O, Bailat C, Duclos F, et al. Treatment of a first patient with FLASH-radiotherapy. Radiother Oncol. 2019; 139:18–22. [PubMed: 31303340]
16. Buonanno M, Grilj V, Brenner DJ. Biological effects in normal cells exposed to FLASH dose rate protons. Radiother Oncol 2019; 139:51–5. [PubMed: 30850209]
17. Schmid TE, Dollinger G, Hable V, Greubel C, Zlobinskaya O, Michalski D, et al. Relative biological effectiveness of pulsed and continuous 20 MeV protons for micronucleus induction in 3D human reconstructed skin tissue. Radiother Oncol. 2010; 95(1):66–72. [PubMed: 20347168]
18. Zlobinskaya O, Siebenwirth C, Greubel C, Hable V, Hertenberger R, Humble N, et al. The effects of ultra-high dose rate proton irradiation on growth delay in the treatment of human tumor xenografts in nude mice. Radiat Res. 2014; 181(2):177–83. [PubMed: 24524347]
19. Matsuura T, Egashira Y, Nishio T, Matsumoto Y, Wada M, Koike S, et al. Apparent absence of a proton beam dose rate effect and possible differences in RBE between Bragg peak and plateau. Med Phys. 2010; 37(10):5376–81. [PubMed: 21089773]
20. Grilj V, Buonanno M, Welch D, Brenner DJ. Proton Irradiation platforms for preclinical studies of high-dose-rate (FLASH) effects at RARAF. Radiat Res. 2020; 194(6):646–55. [PubMed: 32926735]
21. Paganetti H Relative biological effectiveness (RBE) values for proton beam therapy. Variations as a function of biological endpoint, dose, and linear energy transfer. Phys Med Biol. 2014; 59(22):R419–72. [PubMed: 25361443]
22. Weiss H, Epp ER, Heslin JM, Ling CC, Santomasso A. Oxygen depletion in cells irradiated at ultra-high dose-rates and at conventional dose-rates. Int J Radiat Oncol Biol Phys. 1974; 26(1):17–29.
23. Favaudon V, Labarbe R, Limoli CL. Model studies of the role of oxygen in the FLASH effect. Med Phys. 2021.
24. Wilson JD, Hammond EM, Higgins GS, Petersson K. Ultra-high dose rate (FLASH) radiotherapy: Silver bullet or fool's gold? Front Oncol. 2020; 9(1563).
25. Devasagayam TP, Tilak JC, Boloor KK, Sane KS, Ghaskadbi SS, Lele RD. Free radicals and antioxidants in human health: current status and future prospects. JAPI. 2004; 52:794–804. [PubMed: 15909857]
26. Liu SX, Davidson MM, Tang X, Walker WF, Athar M, Ivanov V, et al. Mitochondrial damage mediates genotoxicity of arsenic in mammalian cells. Cancer Res. 2005; 65(8):3236–42. [PubMed: 15833855]
27. Chan DC. Mitochondria: dynamic organelles in disease, aging, and development. Cell. 2006; 125(7):1241–52. [PubMed: 16814712]
28. Su Y-C, Qi X Impairment of mitochondrial dynamics: a target for the treatment of neurological disorders? Future Neurol. 2013; 8(3):333–46.
29. James DI, Parone PA, Mattenberger Y, Martinou JC. hFis1, a novel component of the mammalian mitochondrial fission machinery. The Journal of biological chemistry. 2003; 278(38):36373–9. [PubMed: 12783892]
30. Otera H, Wang C, Cleland MM, Setoguchi K, Yokota S, Youle RJ, et al. Mff is an essential factor for mitochondrial recruitment of Drp1 during mitochondrial fission in mammalian cells. J. Cell Biol. 2010; 191(6):1141–58. [PubMed: 21149567]

31. Palmer CS, Osellame LD, Laine D, Koutsopoulos OS, Frazier AE, Ryan MT. MiD49 and MiD51, new components of the mitochondrial fission machinery. EMBO reports. 2011; 12(6):565–73. [PubMed: 21508961]
32. Guo X, Sesaki H, Qi X. Drp1 stabilizes p53 on the mitochondria to trigger necrosis under oxidative stress conditions in vitro and in vivo. Biochem. 2014; 461(1):137–46.
33. Colvett RD, Rohrig N, Marino SA. Charged particle beams for radiobiology at RARAF. United States; 1977. Contract No.: COO–3243–6.
34. Marino SA. 50 Years of the Radiological Research Accelerator Facility (RARAF). Radiat Res. 2017; 187(4):413–23. [PubMed: 28140790]
35. Grilj V, Brenner DJ. LET dependent response of GafChromic films investigated with MeV ion beams. Phys Med Biol. 2018; 63(24):245021. [PubMed: 30524014]
36. Valente AJ, Maddalena LA, Robb EL, Moradi F, Stuart JA. A simple ImageJ macro tool for analyzing mitochondrial network morphology in mammalian cell culture. Acta histochem. 2017; 119(3):315–26. [PubMed: 28314612]
37. Zhang B, Davidson MM, Zhou H, Wang C, Walker WF, Hei TK. Cytoplasmic irradiation results in mitochondrial dysfunction and DRP1-dependent mitochondrial fission. Cancer Res. 2013; 73(22):6700–10. [PubMed: 24080278]
38. Zhang B, Davidson MM, Hei TK. Mitochondria regulate DNA damage and genomic instability induced by high LET radiation. Life Sci Space Res. 2014; 1:80–8.
39. Zhang S, Wen G, Huang SX, Wang J, Tong J, Hei TK. Mitochondrial alteration in malignantly transformed human small airway epithelial cells induced by alpha-particles. Int J Cancer. 2013; 132(1):19–28. [PubMed: 22644783]
40. Fink SL, Cookson BT. Apoptosis, pyroptosis, and necrosis: mechanistic description of dead and dying eukaryotic cells. Infect Immun. 2005; 73(4):1907–16. [PubMed: 15784530]
41. Cassidy-Stone A, Chipuk JE, Ingerman E, Song C, Yoo C, Kuwana T, et al. Chemical inhibition of the mitochondrial division dynamin reveals its role in Bax/Bak-dependent mitochondrial outer membrane permeabilization. Dev Cell. 2008; 14(2):193–204. [PubMed: 18267088]
42. Adrian G, Konradsson E, Lempart M, Bäck S, Ceberg C, Petersson K. The FLASH effect depends on oxygen concentration. Br J Radiol. 2020; 93(1106):20190702. [PubMed: 31825653]
43. Adrian G, Konradsson E, Beyer S, Wittrup A, Butterworth KT, McMahon SJ, et al. Cancer cells can exhibit a sparing FLASH effect at low doses under normoxic. Front Oncol. 2021; 11:686142. [PubMed: 34395253]
44. Azzam EI, Jay-Gerin JP, Pain D. Ionizing radiation-induced metabolic oxidative stress and prolonged cell injury. Cancer Lett. 2012; 327(1–2):48–60. [PubMed: 22182453]
45. Cheng Y, Ren X, Gowda AS, Shan Y, Zhang L, Yuan YS, et al. Interaction of Sirt3 with OGG1 contributes to repair of mitochondrial DNA and protects from apoptotic cell death under oxidative stress. Cell Death Dis. 2013; 4:e731. [PubMed: 23868064]
46. Zhou X, Li N, Wang Y, Wang Y, Zhang X, Zhang H. Effects of X-irradiation on mitochondrial DNA damage and its supercoiling formation change. Mitochondrion. 2011; 11(6):886–92. [PubMed: 21835270]
47. Liesa M, Palacin M, Zorzano A. Mitochondrial dynamics in mammalian health and disease. Physiol Rev. 2009; 89(3):799–845. [PubMed: 19584314]
48. Tilokani L, Nagashima S, Paupe V, Prudent J. Mitochondrial dynamics: overview of molecular mechanisms. Essays Biochem. 2018; 62(3):341–60. [PubMed: 30030364]
49. Wu J, Zhang B, Wuu YR, Davidson MM, Hei TK. Targeted cytoplasmic irradiation and autophagy. Mutat Res. 2017; 806:88–97. [PubMed: 28283188]
50. Gomes LC, Di Benedetto G, Scorrano L. During autophagy mitochondria elongate, are spared from degradation and sustain cell viability. Nat Cell Biol. 2011; 13(5):589–98. [PubMed: 21478857]
51. Cribbs JT, Strack S. Reversible phosphorylation of Drp1 by cyclic AMP-dependent protein kinase and calcineurin regulates mitochondrial fission and cell death. EMBO reports. 2007; 8(10):939–44. [PubMed: 17721437]
52. Chang CR, Blackstone C. Cyclic AMP-dependent protein kinase phosphorylation of Drp1 regulates its GTPase activity and mitochondrial morphology. JBC. 2007; 282(30):21583–7.

53. Amundson SA. Functional genomics in radiation biology: A gateway to cellular systems-level studies. Radiat Environ Biophys. 2008; 47(1):25–31. [PubMed: 17973116]

54. Han J, Mei Z, Lu C, Qian J, Liang Y, Sun X, et al. Ultra-high dose rate FLASH irradiation induced radio-resistance of normal fibroblast cells can be enhanced by hypoxia and mitochondrial dysfunction resulting from loss of cytochrome C. Front Cell Dev Biol. 2021; 9:672929. [PubMed: 33996831]

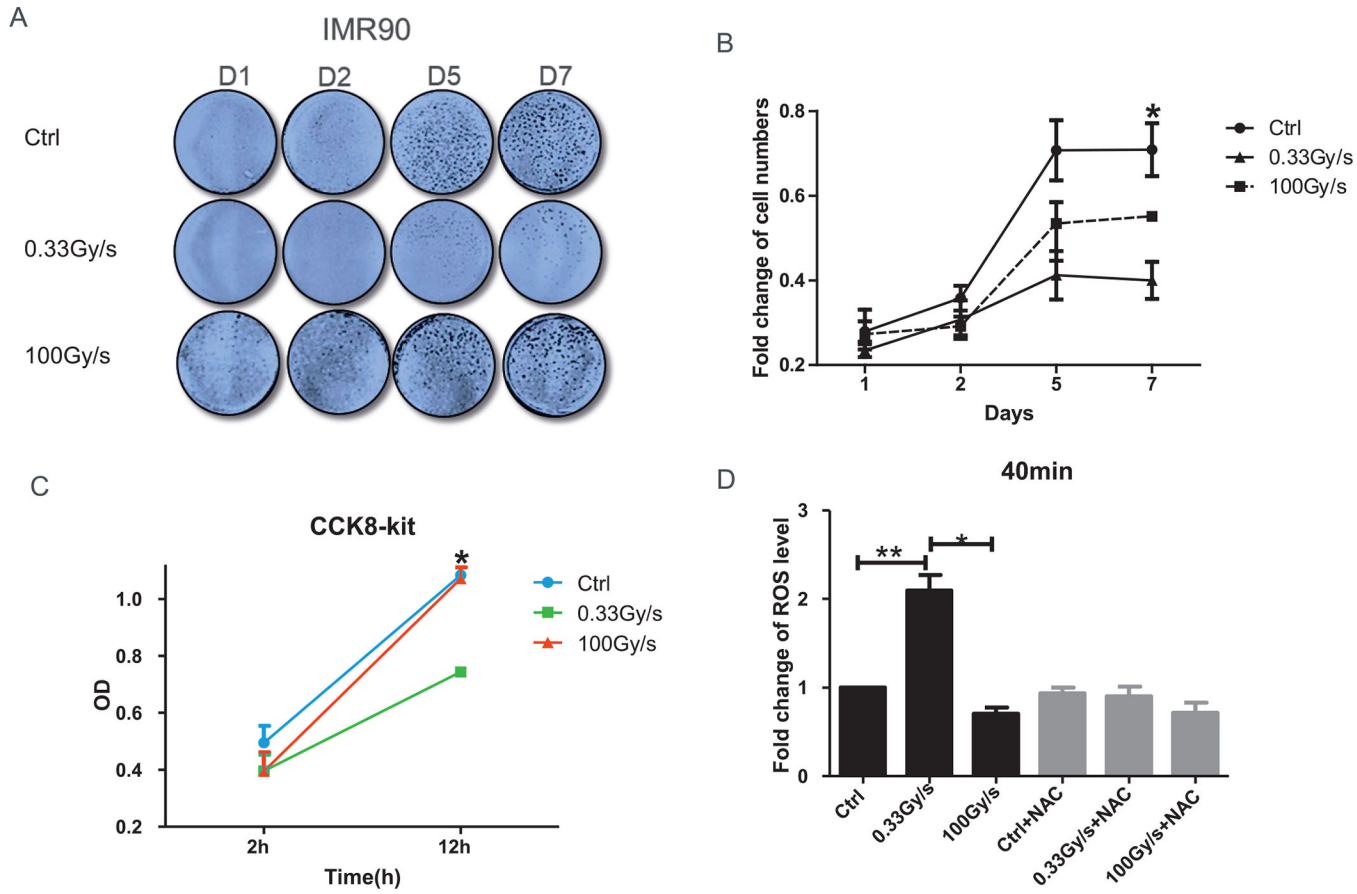

FIG. 1.

Effect of proton-FLASH-RT on normal cellular growth and ROS level. Panels A and B: Viability of IMR90 cells exposed to 15 Gy protons delivered at either 0.03 Gy/s or 100 Gy/s and fixed up to day 7 postirradiation. Panel C: Cell proliferation determined by CCK-8 at either 2 h or 12 h postirradiation. Panel D: CM-H2DCFDA level change, relative to control, after 15 Gy proton irradiation delivered at 0.03 Gy/s or 100 Gy/s and assayed 40 min or 24 h postirradiation with or without N-Acetyl-L-cysteine (NAC). *$P \leq 0.05$; **$P \leq 0.01$. For each sample, three replicates were analyzed and three independent experiments were performed.

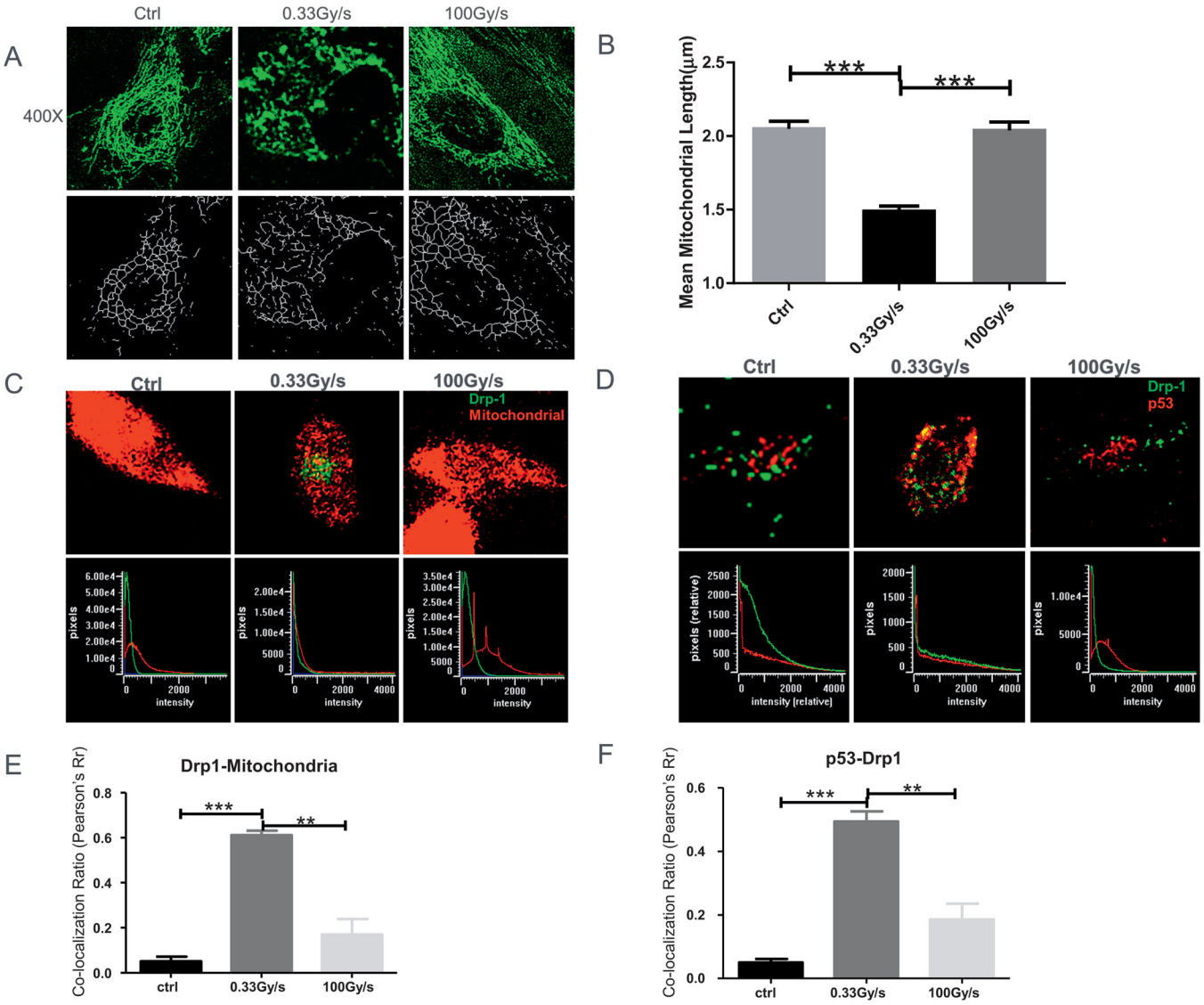

FIG. 2.

Changes in mitochondrial dynamics in response to proton FLASH-RT. Panel A: Representative mitochondrial morphology in normal IMR90 cells stained with Mitotracker Green (100 nM, 400×) 1 h postirradiation (top row). Image analysis was conducted on the "skeletonized" conversion (bottom row). Panel B: Quantification of mitochondrial length. Panel C: Co-localization (defined as overlap between the two signals at the pixel level as seen in the bottom row) between Drp-1 [secondary Alexa488 (green) against anti-Drp1] and mitochondria (MitoTracker Red). Panel D: Co-localization between Drp-1 [secondary Alexa488 (green) against anti-Drp1] and p53 [secondary Alexa555 (red) against anti-p53]. Panel E: Quantification of panel C. Panel E: Quantification of panel D. $^{**}P \leq 0.01$; $^{***}P \leq 0.001$. For each independent experiment (n = 3), at least 50 cells were scored per treatment group for quantification of mitochondrial length and at least 20 cells for co-localization analysis.

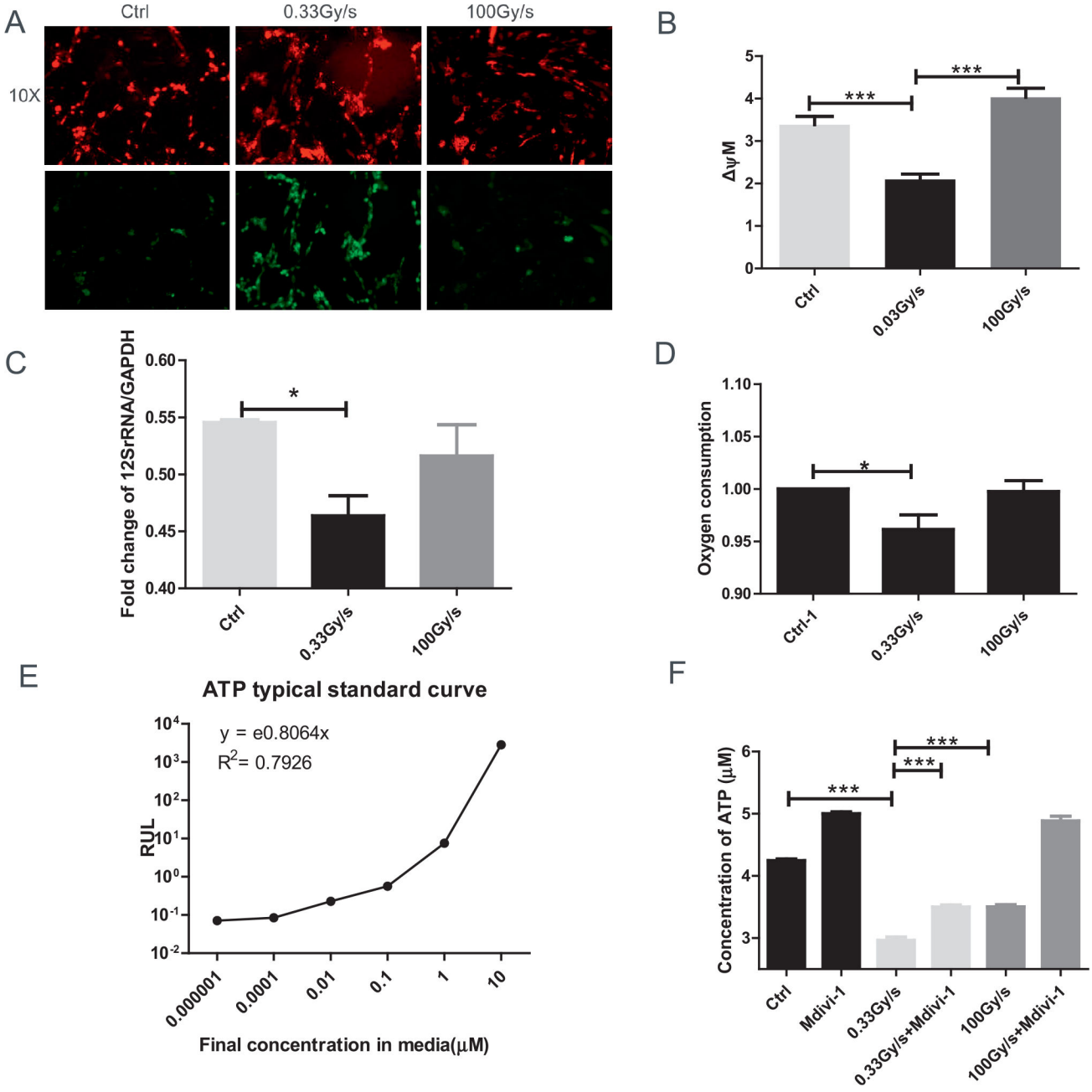

FIG. 3.

Effect of FLASH-RT on mitochondrial functions of normal cells. Panel A: Representative images of control or proton irradiated IMR90 cells delivered at 0.03 Gy/s or 100 Gy/s and stained with JC-1 (20 min at 37°C). Images are shown 200× at 590 nm (top panel) and at 530 nm (bottom panel). Panel B: Quantification of JC-1 stain (red/green fluorescence) indicative of mitochondrial membrane potential (MMP). For each sample, we acquired 5 fields of view (10×). Panel C: Fold change of mitochondrial copy number determined by real time PCR of 12S rRNA/GAPDH (24–48 h). Panel D: Oxygen consumption. Panels E and F: Total levels of cellular ATP (with typical standard curve) were analyzed immediately after

irradiation. *$P \leq 0.05$; ***$P \leq 0.001$. For each endpoint we performed three independent experiments.

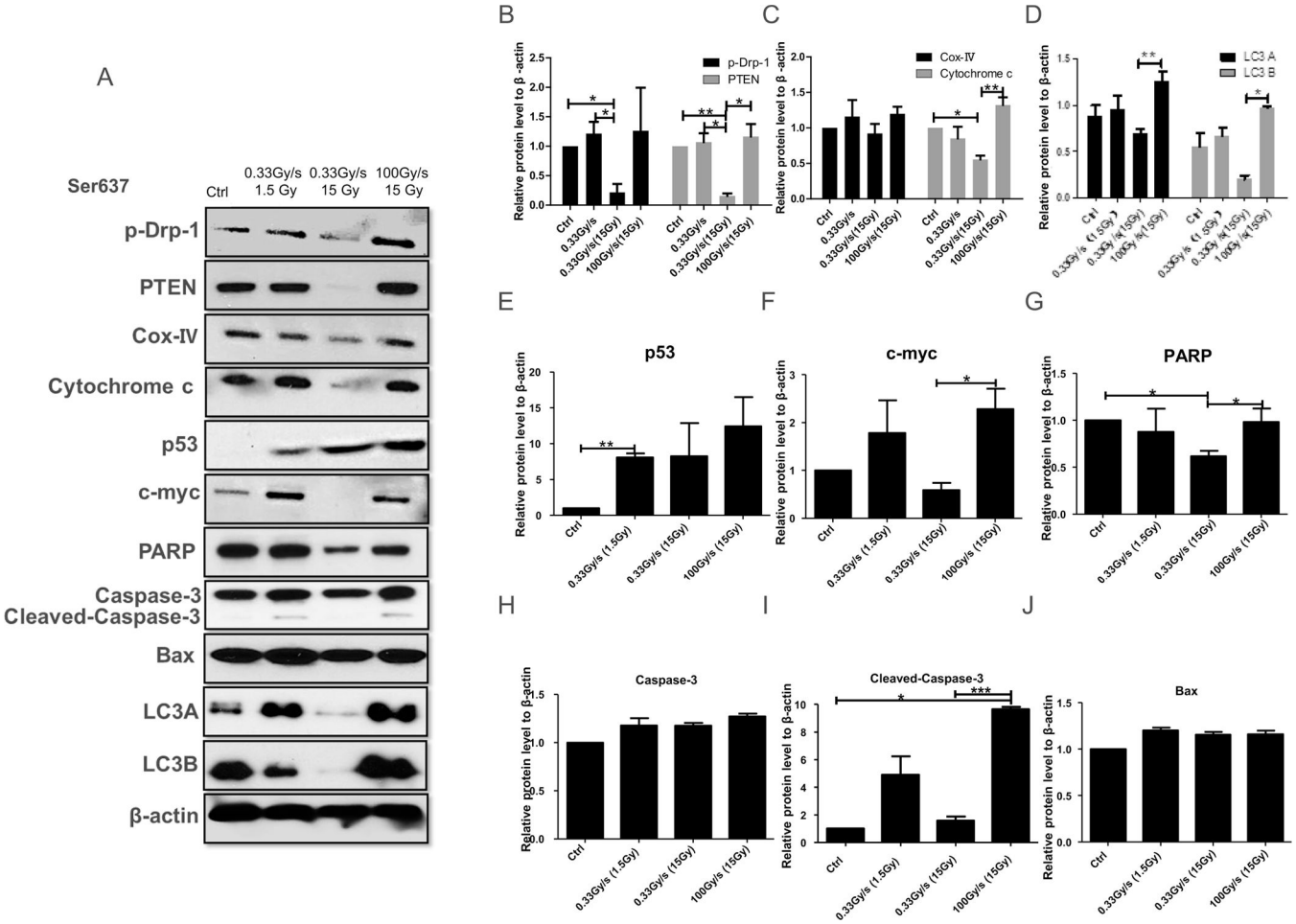

FIG. 4.

Dependence of protein expression by the proton dose rate in normal cells. Panel A: Western blot analyses of proteins related to mitochondrial functions 24 h after 1.5 or 15 Gy proton irradiation delivered at 0.03 Gy/s or 15 Gy delivered at 100 Gy/s. Panels B–J: Quantification of p-Drp-1; PTEN; cytochrome c; cox-IV; LC3A and LC3B; p53; c-myc; PARP; Caspase-3; cleaved-Caspase-3 and Bax, respectively. $*P \leq 0.05$; $**P \leq 0.01$; $***P \leq 0.001$. For each protein we performed three independent experiments.

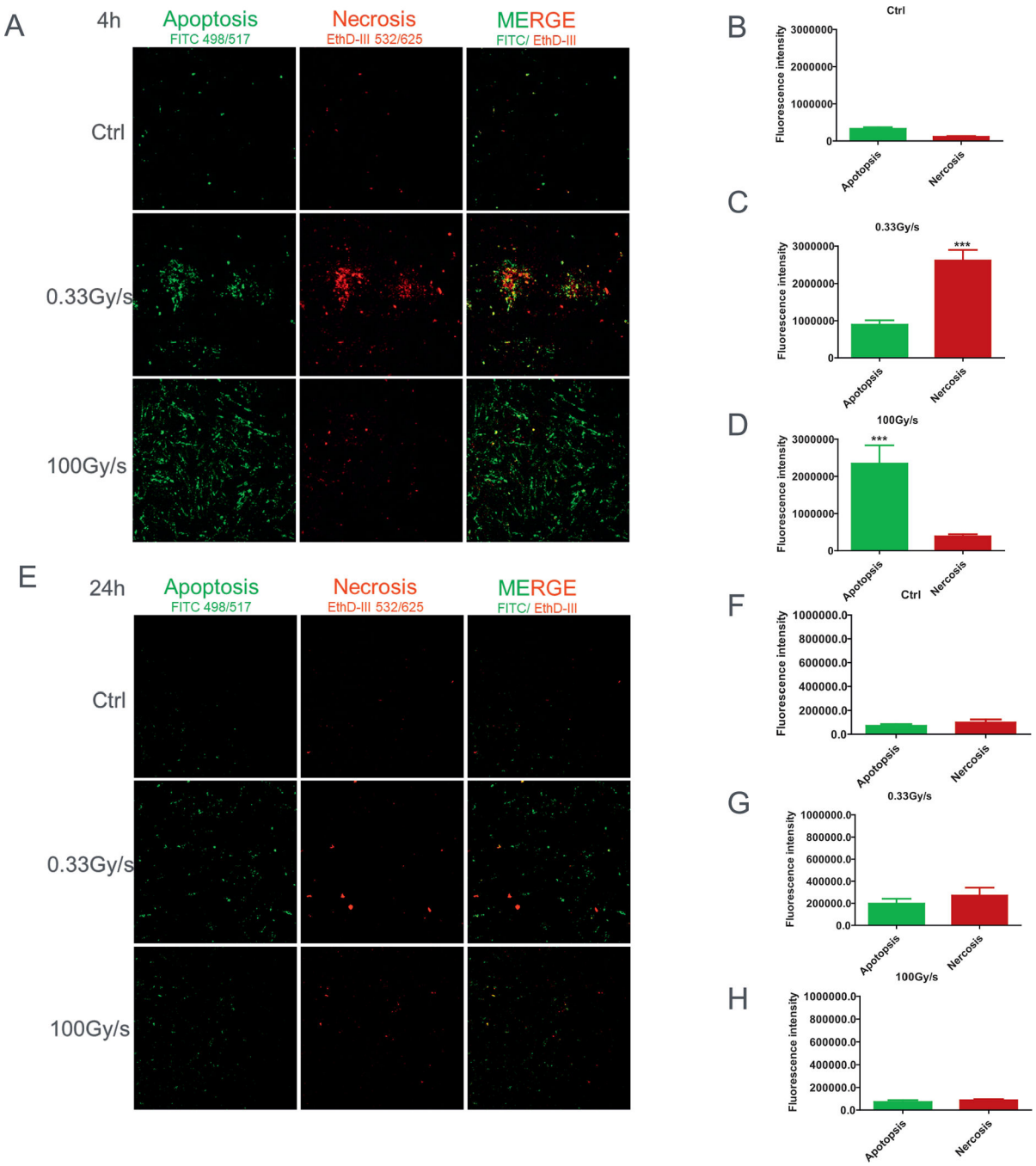

FIG. 5.

The fate of proton-irradiated normal cells delivered at different dose rates. Panel A: Representative images of controls (Ctrl) or proton-irradiated cells delivered at 0.03 Gy/s or 100 Gy/s, analyzed at 4 h postirradiation, stained with AnnV/ EtD-III for 20 min. Typical fluorescence images of FITC-Texas Red or Cy3 filter sets at 200×. Apoptotic cells (green) and necrotic cells (red). Panels B–D: Quantification of AnnV/EtD-III stain (red/ green fluorescence). Panels E–H: Apoptosis and necrosis level change, relative to control, after 15 Gy proton irradiation delivered at 0, 0.03 Gy/s or 100 Gy/s and assayed at 24 h

postirradiation. ***$P \leq 0.001$. For each independent experiment (n = 3), the images of at least 10 randomly selected fields of view were analyzed per each treatment group.

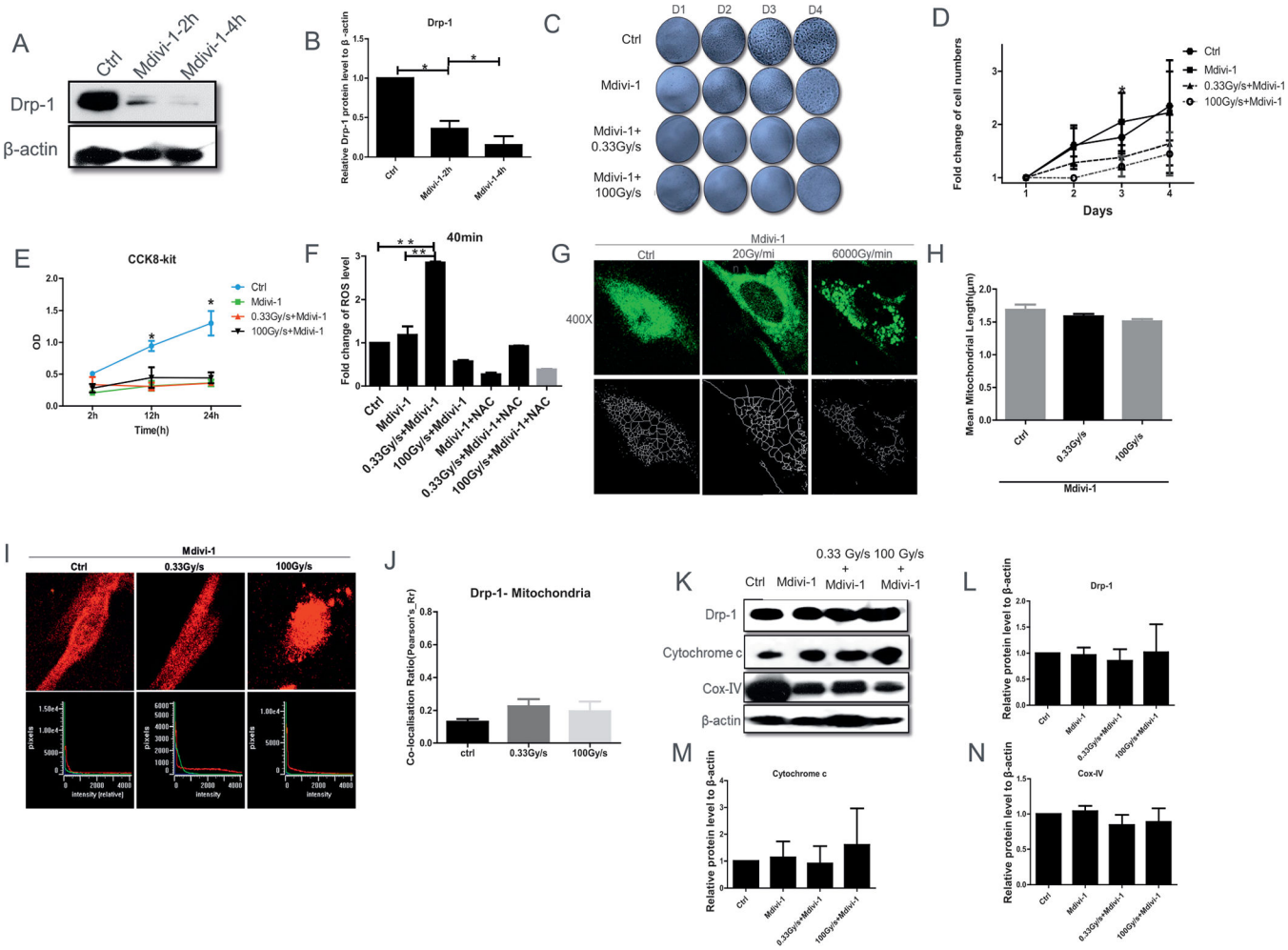

FIG. 6.

FLASH-RT leads to mitochondrial dysfunction in normal cells after inhibition of Drp-1 by Mdivi-1. Panel A: Representative Drp-1 protein level 2 or 4 h after Mdivi-1 treatment with (panel B) quantification. Panels C and D: Relative cell viability after pretreatment of Mdivi-1, up to 4 days after 15 Gy proton irradiation delivered at 0.03 Gy/s or 100 Gy/s. Panel E: CCK-8 assay revealed that FLASH-RT had no protective impact on cell proliferation after pretreatment of Mdivi-1. Panel F: CM-H2DCFDA level change, relative to control, 40 min after 15 Gy proton irradiation delivered at 0.03 Gy/s or 100 Gy/s, with and without the antioxidant N-Acetyl-L-cysteine (NAC). Panels G and H: Representative mitochondrial morphology (Mitotracker green staining, 100 nM, 60×) at 1 h postirradiation. Panels I and J: Co-localization (defined as overlap between the two signals at the pixel level as seen in the lower panels) between Drp-1 [secondary Alexa488 (green) against anti-Drp1] and mitochondria (MitoTracker Red). Panels K–N: Representative Western blot of Drp-1, cytochrome c, and cox-IV in normal cells 15 Gy proton irradiated delivered at the dose rates of 0.03 Gy/s or 100 Gy/s with corresponding quantification. $*P \leq 0.05$; $**P \leq 0.01$. For each endpoint we performed three independent experiments.

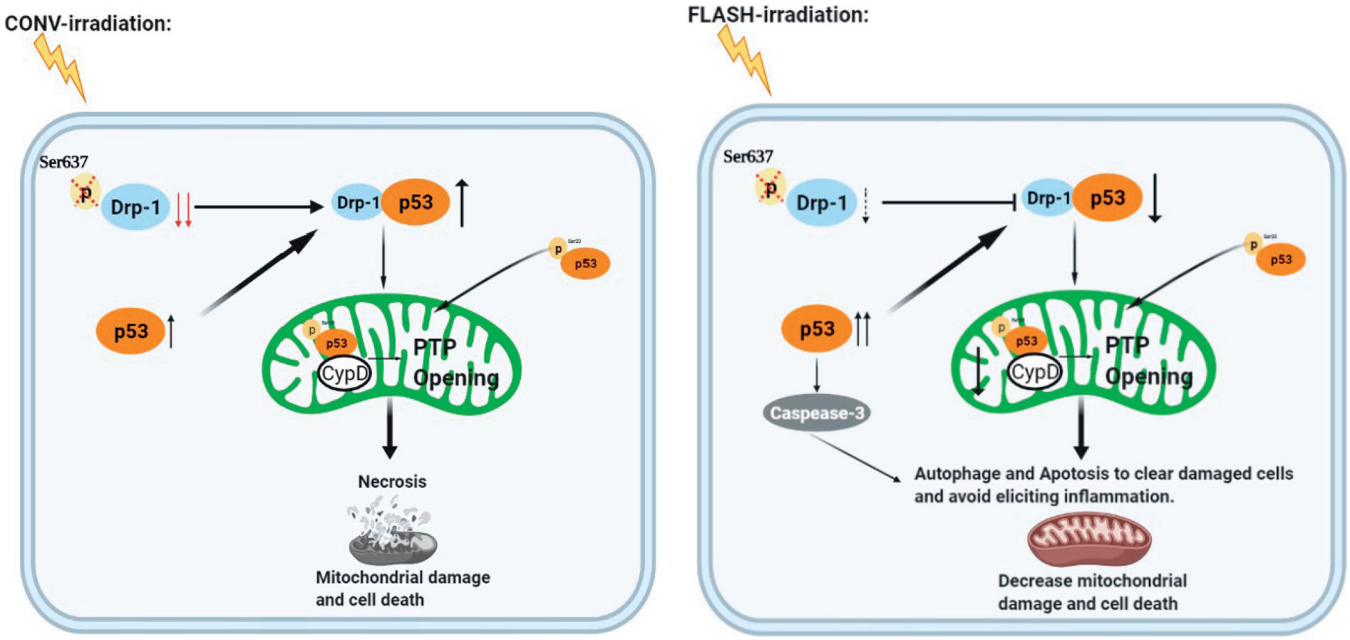

FIG. 7.

Proposed model of the mitochondria-driven mechanisms by which proton-FLASH irradiation can significantly protect the mitochondria from damage including mitochondrial morphology and function via the p53-Drp1 pathway. Exposure of normal cells to conventional-dose protons can make p-Drp1 undergo dephosphorylation with consequent Drp1 translocation into the mitochondria, which may eventually lead to mitochondrion damage and cell death. In contrast, p-Drp1 protein level does not significantly change after exposure to similar proton doses delivered using FLASH-RT. As opposed to protons delivered using FLASH-RT, CONV-RT stimulates the cytoplasmic localization of Drp1 to mitochondria resulting in their dysfunction and fragmentation.